Virtual Impedance Control for Load Sharing and Bus Voltage Quality Improvement

Xiao, Junjie; Wang, Lu; Qin, Zian; Bauer, Pavol

DOI
10.23919/EPE23ECCEEurope58414.2023.10264242

Publication date
2023

Document Version
Final published version

Published in
2023 25th European Conference on Power Electronics and Applications, EPE 2023 ECCE Europe

Virtual Impedance Control for Load Sharing and Bus Voltage Quality Improvement

Junjie Xiao, Lu Wang, Zian Qin and Pavol Bauer
Department of Electrical Sustainable Energy
Delft University of Technology
Delft, The Netherlands
E-Mail: J.Xiao-2@tudelft.nl

***Index Terms*—AC-DC microgrid, Decentralized control structure, Voltage Source Converters (VSCs), Cyber attack, Cyber physical system.**

***Abstract*—This paper proposes a virtual impedance reshaping strategy to share active and harmonic power while promoting the PCC voltage quality. Moreover, the suggested method is resilient to cyber-attacks and immune to communication interruption and delay. Furthermore, it significantly reduces the communication burden. Experiments verify the effectiveness.**

I. Introduction

In a low-voltage microgrid, the droop law (Q-ω, P-V) is commonly utilized for power regulation, given that the feeders exhibit resistive characteristics [1]. While frequency serves as a universal parameter and reactive power can be distributed proportionally [2], achieving proportional sharing of active power poses difficulties due to disparities in line impedance [3]. Microgrid systems often have a proliferation of nonlinear sensitive loads [4], [5], necessitating the fair allocation of harmonic power generated by these loads among the units, which the traditional droop law fails to consider. Numerous approaches have been proposed to tackle these challenges, falling into two main categories: communication-free methods and methods communication-based methods [6]. The virtual impedance technique has proven to be an effective method for achieving precise power-sharing. This approach involves modifying the reference of the voltage controller by incorporating a feedback loop that takes into account the output current. Various studies, such as thosein [1], have demonstrated the effectiveness of this technique. While it possible to compensate for impedance differences by measuring the actual line impedance of each feeder, practical implementation of this approach is often expensive. Some researchers suggest incorporating a substantial virtual impedance into the controller [7]. However, this can introduce significant distortion in the voltage at the Point of Common Coupling (PCC).

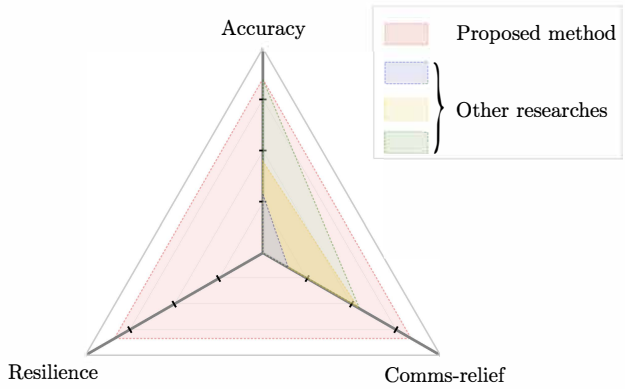

Fig. 1. Comparison of this paper with other studies.

To implement the control methods described in [8] and [9], a Microgrid Central Controller (MGCC) is necessary. The MGCC regulates the virtual impedance based on real-time measurements and power references. However, it is important to note that relying on a central controller makes the system vulnerable to communication failures. The limited availability of communication resources presents a significant obstacle to the distributed control of microgrid systems, resulting in suboptimal system performance [10]. Previous research has suggested periodic data exchange between neighbouring agents as a way to alleviate the communication burden [11], [12]. Another approach involves using discrete-time communication mechanisms to update the states of neighbouring agents, which has shown promise in conserving communication resources [13]. Furthermore,

the Event-Triggered Control (ETC) method, which relies on communication, has gained popularity for intelligent scheduling of communication networks [3]. However, it's important to acknowledge that the communication burden remains challenging, and the adopted communication methods are susceptible to cyber attacks [14] [15], which can have significant implications for control accuracy and system stability [16].

This paper proposes an adaptive virtual impedance technology for harmonic and active power proportionally sharing in an inverter-connected system to cope with the above-mentioned issues. The main contributions of this paper are summarized as follows: 1) The proposed method relaxes the knowledge of the feeder. 2) The adaptive tuning virtual impedance method proposed in this paper can reduce the voltage drop across the impedance. 3) The proposed control strategy can significantly reduce the communication burden. 4) The suggested method in this paper immunizes against communication interruption, delays, and cyber attacks. 5) The proposed methods are validated in load switching and plug-and-play scenarios.

II. Island microgrid control

Fig.2 illustrates a diagram of islanded microgrids that consist of different types of loads, containing linear and nonlinear loads. The participating agents are connected to the AC bus through an LC filter and a feeder. The LC filter is composed of an inductor and a capacitor, which are identified as L_f and C_f, respectively. The feeder behaves as a resistor. The current flowing through the filter inductor is denoted as $i_{L,i}$, while the voltage across the capacitor is represented by $V_{C,i}$. Additionally, the output current of DGi is indicated as $i_{o,i}$.

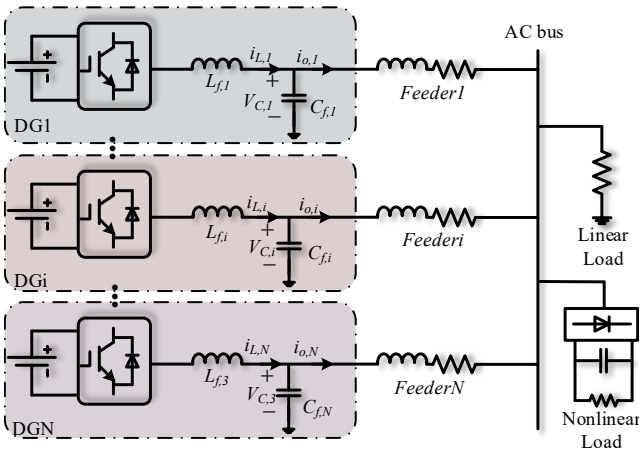

Fig. 2. The scheme of a microgrid with N inverters.

A. Primary control

Resistor-dominant systems commonly employ the P-V and Q-ω droop laws to control power flow. These laws, represented by equations (1) and (2), respectively, are widely adopted:

$$\omega_i = \omega^* + n_{qi}Q_i. \tag{1}$$

$$V_i = V^* - m_{pi}P_i. \tag{2}$$

In the P-V droop law described by (1), ω_i and V_i represent the frequency and voltage amplitude, respectively.

The variables ω^* and V^* indicate the nominal set points for frequency and voltage amplitude, while P_i and Q_i correspond to the calculated active power and reactive power of the ith distributed generator (DG). To ensure proportional power sharing, the droop coefficients m_{pi} and n_{qi} should be inversely set according to the maximum power rating of the DGs. In (1), since ω_i represents a global variable, the output frequency among the participating converters is synchronized, enabling proportional sharing of active power, where $n_{Q1}Q_1 = n_{Q2}Q_2 = \cdots = n_{qi}Q_i$. However, achieving precise active power sharing is challenging due to discrepancies in feeder impedance, which will be discussed in detail in Section II-B.

The reference value for the inner controller, managing the actual output voltage of the filter capacitor, is derived from the droop control results. This reference value is expressed as (3).

$$V_{d,i} = V_i \sin(\int \omega_i \, dt) \tag{3}$$

The inner control is usually composed of a voltage controller and a current controller, in which the reference is the output of the droop controller, denoted as $V_{ref,i} = V_{d,i}$. The control block diagram of the inner loop controller can be equivalent to (4).

$$V_C = V_{ref} \cdot G_V(s) - Z_o(s) \cdot i_o \tag{4}$$

The inner controller's voltage gain is represented by $G_V(s)$ in equation (3), and it is expected to be ideally equal to 1 for a converter. The equivalent impedance of the inverter, denoted as $Z_o(s)$, is determined by the parameters of the voltage controller and the droop coefficient. This impedance influences the overall behavior of the system.

B. Active power analysis

In this section, we examine the impact of mismatched impedances of individual DGs on the inaccurate sharing of active power, as depicted in Figure 3. The voltage drop across the feeder, as described in [3], can be approximately computed using equation (5):

$$\Delta V_i \approx \frac{X_i Q_i + R_i P_i}{V_C} \tag{5}$$

where X_i and R_i represent the inductive and resistive components of the feeder and inverter modeling, ΔV_i denotes the voltage drop.

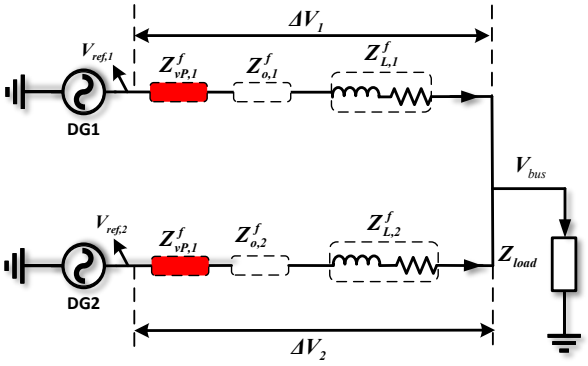

Fig. 3. The effect of feeder mismatch on reactive power sharing

Fig.3 illustrates the representation of various impedances. The values $Z^f_{o,1}$ and $Z^f_{o,2}$ correspond to the modeling impedance, while $Z^f_{L,1}$ and $Z^f_{L,2}$ represent the line impedance of feeder 1 and feeder 2, respectively, as shown in Fig.1. Additionally, $Z^f_{vP,1}$ and $Z^f_{vP,2}$ indicate the virtual impedance used for active power sharing. In a system where resistors dominate, meaning $R_i \gg X_i$, the power flow through the line resistance leads to a voltage drop. This voltage drop can be mathematically expressed as:

$$\Delta V_i \approx \frac{R_i P_i}{V_C} \tag{6}$$

Hence, to ensure proportional sharing of active power, the voltage drop across the participating units needs to be regulated. This can be achieved by appropriately configuring the virtual impedance of each unit to maintain proportionality.

C. Harmonic analysis

To achieve proportional distribution of harmonic power based on the maximum output power capacity, the following conditions must be met.

$$b_1 P^h_{o,1} = b_2 P^h_{o,2} = \cdots = b_i P^h_{o,i} \tag{7}$$

The inverse of the maximum output harmonic power is denoted by b_i, while $P^h_{o,i}$ represents the h-th harmonic power. Fig.4 shows the equivalent circuit of the inverter system operating at the h-th harmonic frequency with a nonlinear load. It is worth noting that the nonlinear load can be treated as a current source, specifically denoted as i^h_{load} [17]. The modeling impedance at the h-th harmonic frequency is given by $Z^h_{o,1}$ and $Z^h_{o,2}$ in equation (4). Additionally, $Z^h_{L,1}$ and $Z^h_{L,2}$ represent the harmonic line impedance of feeder. The mismatch in impedance

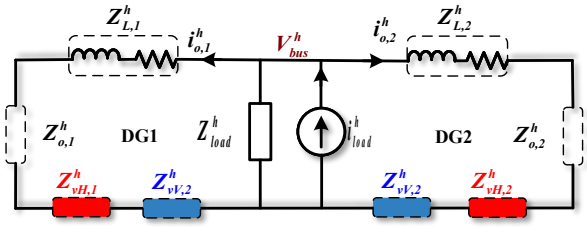

Fig. 4. (a) The effect of feeder mismatch on harmonic current sharing and harmonic voltage control.

between $DG1$ and $DG2$ results in incorrect sharing of harmonic current, as shown in Fig.4, due to the considerably larger h-th order load harmonic impedance Z^h_{load} compared to the equivalent impedance Z^h_{eq} of the DGs. However, by appropriately constructing virtual harmonic impedance $Z^h_{vH,1}$ and $Z^h_{vH,2}$, as illustrated in (10), harmonic sharing can be achieved for selected frequencies.

$$i^h_{o,1}(Z^h_{o,1}+Z^h_{vH,1}+Z^h_{L,1}) = i^h_{o,2}(Z^h_{o,2}+Z^h_{vH,2}+Z^h_{L,2}) \tag{8}$$

D. Bus voltage compensation analysis

The bus voltage at a specific harmonic frequency is influenced by both the harmonic currents generated by the nonlinear load and the equivalent impedance of each inverter. The h-th harmonic voltage at the bus can be mathematically described by (9).

$$V^h_{PCC} = i^h_{o,1} Z^h_{eq,1} = i^h_{o,2} Z^h_{eq,2} \tag{9}$$

The (11) illustrate that the bus voltage harmonic V^h_{PCC} can be reduced by adjusting the virtual impedance Zv, i^h of the DGs, as depicted in Fi.g4. The virtual impedance includes the modeling impedance, line impedance, and virtual impedance of each individual DG, denoted as $Z^h_{eq,1}$ and $Z^h_{eq,2}$ for $DG1$ and $DG2$, respectively.

III. Proposed Impedance Reshape Method

In this study, an adaptive virtual impedance approach is proposed to enhance the quality of bus voltage

while ensuring proportional sharing of harmonic power and active power, as depicted in Fig.5. This approach involves the independent and adaptive adjustment of virtual impedance, thereby reducing the need for precise identification of line impedance. The proposed solution assumes that each unit shares information only with the near inverters, minimizing the communication burden. It is important to note that during the initial stage of system construction, the controller communicates data with its neighboring units. This significantly further reduces the communication requirements. Additionally, auxiliary controllers are designed to improve system resilience and effectively withstand cyber-attacks from the communication network.

A. Sparse communication network

In order to depict the communication network among the involved converters, an undirected cyber graph is considered. This graph represents the data sharing between the local i-th converter of the microgrid and its neighboring converters, denoted as j. The communication graph can be represented as a digraph using edges and links, which can be expressed through a communication adjacency matrix $A = (a_{ij})_{N\times N}$.

The communication weight, denoted as a_{ij}, is set to 1 if the i-th unit and the j-th unit are in regular communication, and 0 otherwise. The degree of the vertex ζ_i is calculated as the sum of the elements in the i-th row of matrix A, given by $d_i = \sum_{j=1}^{N} a_{ij}$. The degree matrix $D = diag(d_1, \cdots, d_N)$ is constructed based on these degrees. Furthermore, the Laplacian matrix L of the communication network is defined as the difference between the degree matrix D and the communication adjacency matrix A, that is, $L = D - A$.

B. Harmonic extract and power calculation

In this study, we employ the multi second-order generalized integrator (SOGI) technique presented in [18] to accurately determine the harmonic current $i_o^h(t)$ and harmonic voltage $V_{bus}^h(t)$. The hth harmonic power of the ith inverter is calculated based on the root mean square (RMS) value $V_{i,rms}$ of the fundamental voltage, the RMS value of harmonic current $i_{o,irms}^h$ and its conjugated signal $i_{o,d}^h$ as (10). Where $V_{i,rms}$=$V_i/\sqrt{2}$.

$$P_i^h = V_{i,rms} i_{o,irms}^h = \frac{1}{2} V_i \sqrt{i_{o,i}^h + i_{o,id}^h} \tag{10}$$

C. Consensus-based control method

Fig.5 illustrates the utilization of the communication network by the participating inverters to exchange information regarding active power, harmonic power, and bus voltage. However, it is important to note that achieving accurate active power sharing does not guarantee optimal harmonic power sharing or the expected bus voltage quality.

Hence, it becomes necessary to independently design controllers for active power sharing, harmonic sharing, and bus voltage compensation. The active power controller can be formulated using equation (11).

$$Z_{vP,i}^f = \int k_{vP,i}^f [\sum_{j\in Ni} a_{ij}(m_{pj}P_j^f - m_{pi}P_i^f)]dt \tag{11}$$

The virtual impedance introduced in (12) can properly share the harmonic power.

$$Z_{vH,i}^h = \int k_{vH,i}^h [\sum_{j\in Ni} a_{ij}(b_j P_j^h - b_i P_i^h)]dt \tag{12}$$

The bus harmonic voltage compensation controller is written as (13).

$$Z_{vV,i}^h = k_{vV,i}^h \int \sum_{j\in Ni} [(D_j^h - D_i^h) + (D_r^h - D_i^h)]dt \tag{13}$$

To mitigate errors in harmonic power sharing, integral controllers are utilized. The parameters $k_{vP,i}^f$, $k_{vH,i}^h$, and $k_{vV,i}^f$ represent the impedance reshaping factors for active power sharing, harmonic power sharing, and harmonic voltage compensation, respectively. The nominal value of harmonic distortion is denoted as D_r^h, while D_i^h represents the h-th order harmonic distortion of the i-th unit, as described in (14).

$$D^h = \frac{V_{bus}^h}{V_{bus}^f} \tag{14}$$

In (14), V_{bus}^f represents the fundamental voltage, while V_{bus}^h represents the voltage at the h-th harmonic. It is important to note that, in low-voltage grids with small line impedance, the capacitor voltage is often used as a substitute for the Point of Common Coupling (PCC) voltage. To share the power and compensate the voltage quality, the virtual impedance is dynamically adjusted to ensure proportional and reasonable fundamental and harmonic impedance.

By incorporating the virtual impedance reshaping loops, the voltage reference for the double-loop voltage controller is obtained using (15):

$$V_{ref} = V_d - Z_{vP}^f i_o^f - Z_{vH}^h i_o^h - Z_{vV}^h i_o^h \tag{15}$$

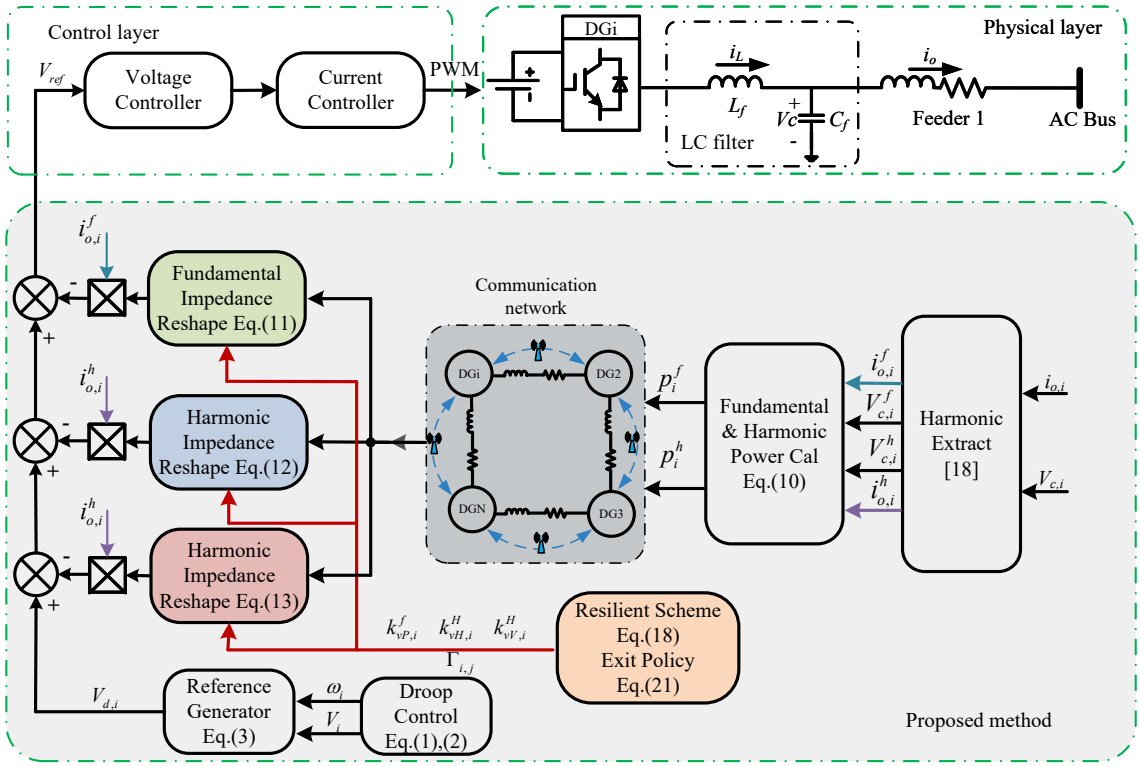

Fig. 5. The proposed virtual impedance framework.

IV. Cyber Attack and Stability Analysis

In order to ensure the accurate configuration of fundamental and harmonic impedances, consensus-based algorithms are commonly employed. However, these methods are vulnerable to cyber-attacks. This section focuses on analysing and modelling a specific cyber-attack known as the false data injection attack (FDIA). We then propose a strategy to challenge the convergence performance of the FDIA. Additionally, we present a cyber-attack mitigation technique aimed at preserving the security of the system.

A. Cyber attack problem statement

The false data injection attack (FDIA) has garnered significant attention among the various types of attacks. In this attack, fake data is deliberately generated, modelled using (16), and then injected into the actual data of the system [19].

$$x_{a,j} = x_j + \eta_j \varepsilon(t) \tag{16}$$

where $x_{a,j}$ represents the information received from the neighboring unit under attack, while x_j represents the actual information without cyber attack, the presence of the false data injection attack (FDIA) is denoted by a binary variable η_j, where $\eta_j = 1$ indicates the presence of an attack, and $\eta_j = 0$ signifies the absence of FDIA. The attack is characterized by a malicious element $\varepsilon(t)$.

B. Resilient framework and exit policy

In this study, we present a resilience-improved controller designed to mitigate the impact of cyber attacks. Our proposed resilience scheme aims to counteract cyber attacks that hinder the convergence of virtual impedance. Specifically, equation (17) represents the formulation of our resilience scheme, with a focus on the active power-sharing controller. It is important to note that this resilience scheme can also be extended to the harmonic power-sharing and harmonic voltage compensation controllers.

$$Z^f_{vP,i} = \int k^f_{vP,i} \sum_{j \in N_i} a_{ij} \Delta\delta dt \tag{17}$$

If we take $\Delta\delta_{i,j} = m_{pj} P^f_j - m_{pi} P^f_i$. $\Delta\delta'_{i,j}$ can be taken as follows to replace the original data:

$$\Delta\delta'_{i,j} = (1 - \Gamma_{i,j}) \Delta\delta_{i,j} \tag{18}$$

where $\Gamma_{i,j}$ is a binary variable, representing the existence of a cyber attack or not.

$$\Gamma_{i,j} = \begin{cases} 1, & if \quad |\Psi_{i,j}| \geq \Upsilon_i \\ 0, & else \end{cases} \tag{19}$$

To identify cyber-attacks, we utilize the variable $\Psi_{i,j}$, which is defined by equation (20). The cyber attack measure threshold is represented by Υ_i, and in this paper, it is defined as $\Upsilon_i = 0.01 m_{pi} P_i^f$. If the absolute value of $\Psi_{i,j}$ is greater than or equal to Υ_i, we set $\Gamma_{i,j} = 1$, indicating the presence of a cyber attack. Conversely, if $|\Psi_{i,j}| < \Upsilon_i$, it suggests the absence of a cyber attack within the system.

$$\Psi_{i,j} = a_{ij}(m_{pj} P_j^f - m_{pi} P_i^f), \forall j \in N_i \tag{20}$$

In the event of a cyber-attack between the j-th and i-th DG units, a binary signal $\Gamma_{i,j} = 0$ is transmitted to isolate the compromised data, ensuring that the infected data is disregarded. As a result, the proposed communication-based strategy within the resilient framework remains resilient against cyber attacks.

In order to reduce the communication burden, an auxiliary controller is used. This controller is intended to disable the proposed method and can be expressed as follows:

$$k_{vP,i}^f = \begin{cases} k_{vP^*,i}^f, & if \quad \Gamma_{i,1} \cup \Gamma_{i,2} \cdots \cup \Gamma_{i,N} = 0 \\ 0, & else \end{cases} \tag{21}$$

Once the inverter system has been established using the proposed method, it is assumed that harmonic and active power can be shared in a nearly proportional manner. This activation triggers the auxiliary controller, causing the impedance reshaping factor $k_{vP,i}^f$ to be set to 0. Consequently, the microgrid becomes independent of communication, as proportional power sharing is maintained without the need for continuous communication.

V. Experiment Results

To validate the effectiveness of the proposed adaptive control strategy, experiments were conducted on a distributed AC microgrid consisting of three inverters connected in parallel, as depicted in Fig.6. The inverters are linked to the AC bus through an LC filter and line impedance.

Following the structure in Fig.6, several cases are carried out in this paper to verify the effectiveness of the proposed adaptive control scheme with different operations. The plant and control parameters of the microgrid are provided in Table I. In this paper, the inverters' output harmonic and active power rate follows the maximum capacity proportion set as 1:2:3. The PCC harmonic voltage disordered rate should be below 5%.

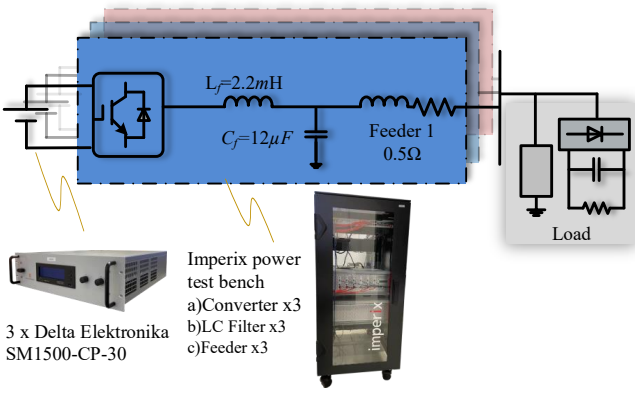

Fig. 6. Experiment setup.

TABLE I
Parameters of the Microgrid in Experiment

Symbol	Interpretation	Value
U_{dc}	DC-link voltage	150V
Z_L	Line impedance	0.5Ω
L_f	Inductor of LC filter	2.2mH
C_f	Capacitor of LC filter	12μH
f_s	Switch frequency	20kHz
m_{P1}, n_{Q1}	Droop coefficient of $DG1$	1/1000
m_{P2}, n_{Q2}	Droop coefficient of $DG2$	1/2000
m_{P3}, n_{Q3}	Droop coefficient of $DG3$	1/3000
k_{ph}	Proportional coefficient	0.001
k_{rh}	resonant coefficient	50
ω^*	Nominal angular frequency	314rad/s
V^*	Nominal voltage amplitude	110V

A. Active and harmonic power sharing

Fig.7 presents the control performance of the proposed method. As it is shown in Fig.7(a),(b), during stage 1, the microgrids are regulated by conventional droop control, which results in improper power sharing. Subsequently, the proposed method is activated, and the active power and $3rd$ harmonic power are proportionally shared. Moreover, in stage 3 and stage 4, communication delay and interruption are intentionally imposed in the network from $DG2$ to $DG1$. Notably, despite these disruptions, the system response exhibits no significant changes, and the proposed method maintains accurate power sharing.

B. Cyber attack and resilience enhancement

Fig.7(c) and (d) demonstrate the impact of cyber attacks on microgrids and the effectiveness of the proposed method in mitigating such attacks. In the beginning, no cyber attack on the communication network. When it

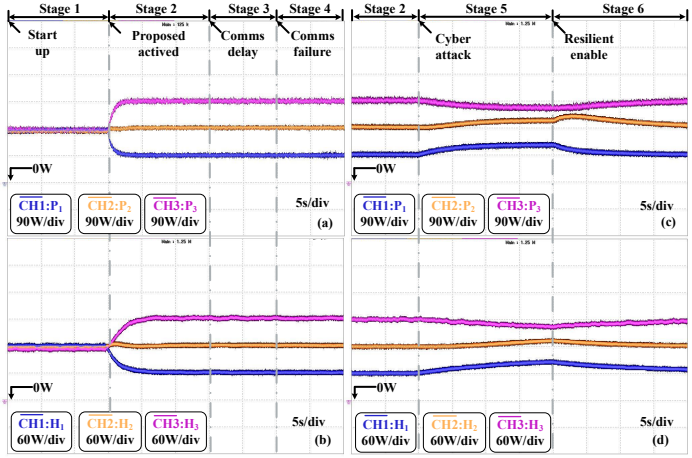

Fig. 7. Experiments performance of the proposed controller: (a), (c): active power; (b), (d): 3rd harmonic power.

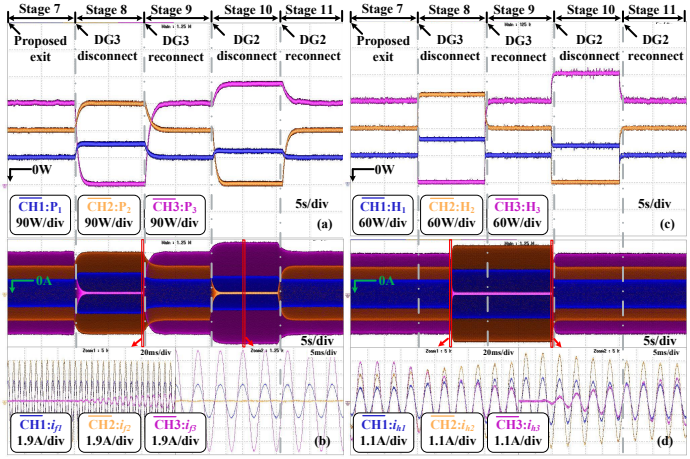

Fig. 8. Experiments performance of the proposed controller: (a), (b): active power and fundamental current; (c), (d): 3rd harmonic power and current.

transits into stage 5, the communication line from $DG2$ to $DG1$ is subject to a false data injection attack with $\varepsilon(t) = 100$ for both the active power and harmonic power controllers. As a result, the power-sharing ratio deviates from the optimal point. In stage 6, the proposed resilient framework is activated, eliminating the corrupted data and recovering the power-sharing ratio to 1:2:3. The results demonstrate the resilience of the proposed method against cyber-attacks, highlighting its potential for enhancing the security and stability of microgrids.

C. Communication relief strategy

The limited communication resource constraints the wide use of distributed control. This paper proposes an exit policy to alleviate the communication burden by disabling the adaptive tunning virtual impedance after the system is built up. Moreover, for all the power-sharing technology, it is necessary to keep sharing accuracy when one DG unit drops out. This paper tests the active and harmonic power in the plug-and-play operation after the communication-based method exit. As shown in Fig.8 , where Fig.8(a),(c) represents the active power and $3rd$ harmonic power performance respectively, while Fig.8(b),(d) denote the corresponding fundamental current and $3rd$ harmonic current.

The communication-based control strategy is terminated at the commencement of stage 7, allowing active and harmonic power to continue proportionally sharing without communication support. In stage 8, $DG3$ disconnects, while the operational $DG1$ and $DG2$ maintain a power-sharing ratio of 1:2. In stage 10, $DG2$ drops out, and the operational $DG1$ and $DG3$ maintain a power-sharing ratio of 1:3. In both cases, the system operates reliably and accurately without the need for communication-based control. During stage 9 and stage 11, the disconnected unit is reconnected, and the system returns to its original configuration. The current waveform in Fig.8(b),(d) demonstrates consistent and accurate power sharing throughout the entire operation.

D. Harmonic voltage compensation

To evaluate the effectiveness of the proposed control, a comparison is made between the waveforms obtained before and after the implementation of the proposed method, as illustrated in Fig.9. At stage 12, the harmonic distortion rate, represented by D_h, is 10%, with the fundamental voltage measured at 98V and the $3rd$ harmonic voltage at 10V. Subsequently, at stage 13, the proposed method is employed, attenuating the $3rd$ harmonic impedance. Consequently, the harmonic distortion rate D_h decreases to 5%, the $3rd$ harmonic voltage shifts to 5V, while the fundamental voltage remains unchanged.

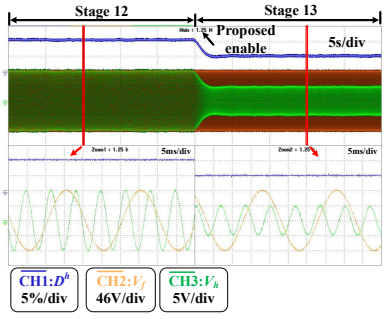

Fig. 9. The validity of PCC harmonic voltage compensation.

VI. Conclusion

This paper proposes an adaptively adjusted virtual impedance method that interacts only with neighbouring units during the system construction phase. This significantly reduces communication time and ensures plug-and-play operation. An auxiliary controller is also employed to isolate corrupted data, thereby enhancing system resilience against cyber-attacks and communication disruptions. Furthermore, harmonic voltage compensation ensures that PCC voltage harmonic distortion remains within 5%. The experimental results verify the performance of the proposed control scheme.

References

[1] J. M. Guerrero, L. G. De Vicuna, J. Matas, M. Castilla, and J. Miret, "Output impedance design of parallel-connected ups inverters with wireless load-sharing control," *IEEE Transactions on industrial electronics*, vol. 52, no. 4, pp. 1126–1135, 2005.

[2] J. Xiao, Y. Jia, B. Jia, Z. Li, Y. Pan, and Y. Wang, "An inertial droop control based on comparisons between virtual synchronous generator and droop control in inverter-based distributed generators," *Energy Reports*, vol. 6, pp. 104–112, 2020.

[3] J. Lu, M. Savaghebi, B. Zhang, X. Hou, Y. Sun, and J. M. Guerrero, "Distributed dynamic event-triggered control for accurate active and harmonic power sharing in modular on-line ups systems," *IEEE Transactions on Industrial Electronics*, 2021.

[4] Z. Qin, L. Wang, and P. Bauer, "Review on power quality issues in ev charging," in *2022 IEEE 20th International Power Electronics and Motion Control Conference (PEMC)*, 2022, pp. 360–366.

[5] L. Wang, Z. Qin, T. Slangen, P. Bauer, and T. van Wijk, "Grid impact of electric vehicle fast charging stations: Trends, standards, issues and mitigation measures - an overview," *IEEE Open Journal of Power Electronics*, vol. 2, pp. 56–74, 2021.

[6] H. Han, X. Hou, J. Yang, J. Wu, M. Su, and J. M. Guerrero, "Review of power sharing control strategies for islanding operation of ac microgrids," *IEEE Transactions on Smart Grid*, vol. 7, no. 1, pp. 200–215, 2015.

[7] J. Chen, L. Wang, L. Diao, H. Du, and Z. Liu, "Distributed auxiliary inverter of urban rail train—load sharing control strategy under complicated operation condition," *IEEE Transactions on Power Electronics*, vol. 31, no. 3, pp. 2518–2529, 2015.

[8] T. V. Hoang and H.-H. Lee, "Accurate power sharing with harmonic power for islanded multibus microgrids," *IEEE Journal of Emerging and Selected Topics in Power Electronics*, vol. 7, no. 2, pp. 1286–1299, 2018.

[9] T. V. Hoang, T. D. Nguyen, and H.-H. Lee, "Adaptive virtual impedance control scheme to eliminate reactive power sharing errors in islanded microgrid," in *2016 IEEE International Conference on Sustainable Energy Technologies (ICSET)*. IEEE, 2016, pp. 224–229.

[10] Y. Fan, G. Hu, and M. Egerstedt, "Distributed reactive power sharing control for microgrids with event-triggered communication," *IEEE Transactions on Control Systems Technology*, vol. 25, no. 1, pp. 118–128, 2016.

[11] J. Zhou, S. Kim, H. Zhang, Q. Sun, and R. Han, "Consensus-based distributed control for accurate reactive, harmonic, and imbalance power sharing in microgrids," *IEEE Transactions on Smart Grid*, vol. 9, no. 4, pp. 2453–2467, 2016.

[12] L. Meng, X. Zhao, F. Tang, M. Savaghebi, T. Dragicevic, J. C. Vasquez, and J. M. Guerrero, "Distributed voltage unbalance compensation in islanded microgrids by using a dynamic consensus algorithm," *IEEE Transactions on Power Electronics*, vol. 31, no. 1, pp. 827–838, 2015.

[13] X. Lu, X. Yu, J. Lai, J. M. Guerrero, and H. Zhou, "Distributed secondary voltage and frequency control for islanded microgrids with uncertain communication links," *IEEE Transactions on Industrial Informatics*, vol. 13, no. 2, pp. 448–460, 2016.

[14] J. Xiao, L. Wang, Z. Qin, and P. Bauer, "Detection of cyber attack in smart grid: A comparative study," in *2022 IEEE 20th International Power Electronics and Motion Control Conference (PEMC)*, 2022, pp. 48–54.

[15] Q. Zhou, M. Shahidehpour, A. Alabdulwahab, and A. Abusorrah, "A cyber-attack resilient distributed control strategy in islanded microgrids," *IEEE Transactions on Smart Grid*, vol. 11, no. 5, pp. 3690–3701, 2020.

[16] J. Xiao, L. Wang, Z. Qin, and P. Bauer, "An adaptive cyber security scheme for ac micro-grids," in *2022 IEEE Energy Conversion Congress and Exposition (ECCE)*. IEEE, 2022, pp. 1–6.

[17] Z. Wang, Y. Chen, X. Li, Y. Xu, W. Wu, S. Liao, H. Wang, and S. Cao, "Adaptive harmonic impedance reshaping control strategy based on a consensus algorithm for harmonic sharing and power quality improvement in microgrids with complex feeder networks," *IEEE Transactions on Smart Grid*, vol. 13, no. 1, pp. 47–57, 2021.

[18] P. Rodríguez, A. Luna, I. Candela, R. Mujal, R. Teodorescu, and F. Blaabjerg, "Multiresonant frequency-locked loop for grid synchronization of power converters under distorted grid conditions," *IEEE Transactions on Industrial Electronics*, vol. 58, no. 1, pp. 127–138, 2010.

[19] J. Xiao, L. Wang, Z. Qin, and P. Bauer, "A Resilience Enhanced Secondary Control for AC Micro-grids," *IEEE Transactions on Smart Grid*, 2023.